SANDIA REPORT

SAND2003-8687
Unlimited Release
Printed January 2004

Fundamental Limitations of LIGA X-Ray Lithography: Sidewall Offset, Slope and Minimum Feature Size

S. K. Griffiths

Prepared by
Sandia National Laboratories
Albuquerque, New Mexico 87185 and Livermore, California 94550

Sandia is a multiprogram laboratory operated by Sandia Corporation, a Lockheed Martin Company, for the United States Department of Energy under Contract DE-AC04-94AL85000.

Sandia National Laboratories

Issued by Sandia National Laboratories, operated for the United States Department of Energy by Sandia Corporation.

Available to DOE and DOE contractors from
Office of Scientific and Technical Information
P.O. Box 62
Oak Ridge, TN 37831

Prices available from (615) 576-8401, FTS 626-8401

Available to the public from
National Technical Information Service
U.S. Department of Commerce
5285 Port Royal Rd
Springfield, VA 22161

NTIS price codes
Printed copy: A03
Microfiche copy: A01

SAND2003-8687
Unlimited Release
Printed January 2004

Fundamental Limitations of LIGA X-Ray Lithography: Sidewall Offset, Slope and Minimum Feature Size

Stewart K. Griffiths
Sandia National Laboratories
Livermore, California 94551-0969

Abstract

Analytical and numerical methods are used to examine photoelectron doses and their effect on the dimensions of features produced by deep x-ray lithography. New analytical models describing electron doses are presented and used to compute dose distributions for several feature geometries. The history of development and final feature dimensions are also computed, taking into account the dose field, dissolution kinetics based on measured development rates, and the transport of PMMA fragments away from the dissolution front. We find that sidewall offsets, sidewall slope and producible feature sizes all exhibit at least practical minima and that these minima represent fundamental limitations of the LIGA process. The minimum values under optimum conditions are insensitive to the synchrotron spectrum, but depend strongly on resist thickness. This dependence on thickness is well approximated by simple analytical expressions describing the minimum offset, minimum sidewall slope, minimum producible size of positive and negative features, maximum aspect ratio and minimum radius of inside and outside corners.

Introduction

The LIGA process [1-3] employs deep x-ray lithography (DXRL) to produce metal or plastic parts having lateral dimensions up to several centimeters, an overall thickness up to a few millimeters, and feature sizes down to one micrometer or somewhat less. To make such parts, a thick PMMA resist is first exposed to synchrotron radiation through a patterned absorber mask. The resist is subsequently developed, yielding a mold that is then filled by electrodeposition to form either individual metal parts or a metal tool for polymer replication by embossing or injection molding. Alternatively, the mold (or a replica) may be filled via casting to produce ceramic or composite parts.

Feature tolerances and the minimum feature size producible by LIGA are limited by many considerations. Most of these, including beam divergence [4,5], fluorescence radiation [4-9], mask thermal deformations [10], development conditions [8,11], feature loss of adhesion [7,8,12-14] and PMMA swelling [15-17], are practical limitations amenable to improvement through optimization, innovation and determined process engineering. In contrast, fundamental limitations are beyond our control as they arise from physical phenomena inherent to x-ray lithography. These phenomena are diffraction, scattering and the emission of electrons

accompanying photon absorption, and each may limit tolerances and producible feature size under certain special conditions [4-6,18-22]. For conditions characteristic of LIGA, however, only electron emission significantly influences developed feature geometry for resist thicknesses greater than about 10 μm and less than several millimeters.

During x-ray exposure of the PMMA resist, primary photons absorbed in the PMMA produce high-energy electrons. As illustrated in Figure 1, these electrons travel in a somewhat random manner, depositing energy as they move, and so can produce unwanted doses in the shadow region under the mask absorber. As a result, the dissolution front encroaches into shadow regions during resist development, yielding fully-developed features having sidewalls that are offset from the mask absorber pattern and sloped sidewall profiles that are not parallel to the x-ray beam. These dimensional discrepancies between the mask pattern and developed features also limit the minimum producible feature size.

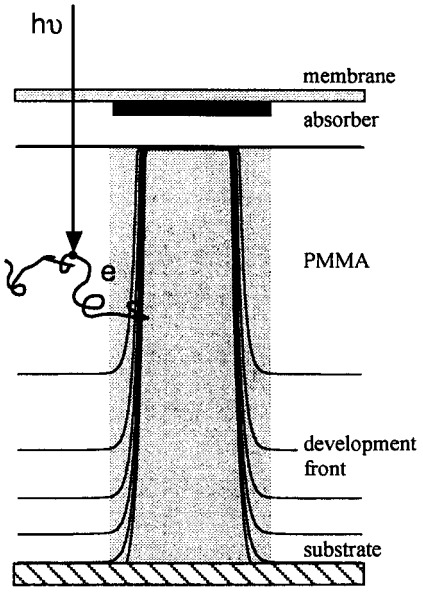

Figure 1. Schematic of x-ray mask and PMMA resist. Photons absorbed in bright regions of the PMMA produce electron doses in the shadow region under the mask absorber. Such doses lead to dimensional errors in the developed feature.

Previous numerical studies, employing both Monte Carlo and approximate methods, have addressed in some detail the distribution of the electron dose near an absorber edge [4,5,18-22] and that surrounding multi-dimensional features [23]. However, there has been relatively little study of the effect of this distribution on the two-dimensional history of development and resulting developed feature geometry. A few previous papers have addressed this aspect of the problem [19,20,23], but these investigations were motivated by microelectronics manufacturing and addressed only soft x-rays and a resist thickness of 1 μm or less. Only two of these efforts [20,23] considered the multi-wavelength x-ray spectrum characteristic of synchrotron radiation.

In the present study, electron dose distributions together with the development history are used to investigate final feature geometries for thick PMMA resists characteristic of LIGA. These dose distributions are computed by means of analytical dose kernels, taking into account the synchrotron spectrum, x-ray transmission through filters and the mask membrane, photon absorption in the resist, and the redistribution of the primary dose by photoelectrons. From these doses, the history of development and final geometry are calculated via a front-tracking

algorithm that advances the dissolution interface in proportion to the local dissolution rate and normal to the local front geometry. The dissolution rate is computed using the local dose, developer temperature and the local concentration of dissolved PMMA fragments.

These computational methods are used to examine four fundamental limitations of LIGA DXRL: minimum sidewall offset from the mask absorber edge; minimum sidewall slope at the mid-height of the resist; the minimum producible size of isolated features; and the minimum producible size of small features patterned onto larger structures. Optimum conditions yielding minimum dimensional errors are discussed, and numerical results under these conditions are presented for a wide range of resist thicknesses and several synchrotron spectra. Simple algebraic expressions approximating producible feature geometries as a function of resist thickness are also presented. These results provide guidelines for the ultimate capabilities of LIGA DXRL, as well a benchmark for assessing practical limitations of the process.

Mathematical Model

Photoelectron dose distributions are computed here using analytical dose kernels, similar in nature to the parametric Gaussian approximation developed by Ocola and Cerrina [21]. These kernels describe electron doses for half-space, plane and line sources, as shown in Figure 2. Such kernels in general describe both photoelectrons and Auger electrons and are accurate for any resist having an effective atomic number less than about 10. The main restriction on their use is that the photon energy must be below about 1 MeV so that pair production is not possible.

Analytical expressions for the three kernel geometries are based on Monte Carlo calculations [24] for a line source in PMMA. The line source kernel was obtained by fitting these numerical results with a simple analytical expression of the correct functional form. Kernels for half-space and plane sources were then obtained by numerical integration of a spatial distribution of line sources, followed again by fitting with expressions of the correct form. From these elemental dose kernels, the dose field can be computed rapidly for any feature geometry.

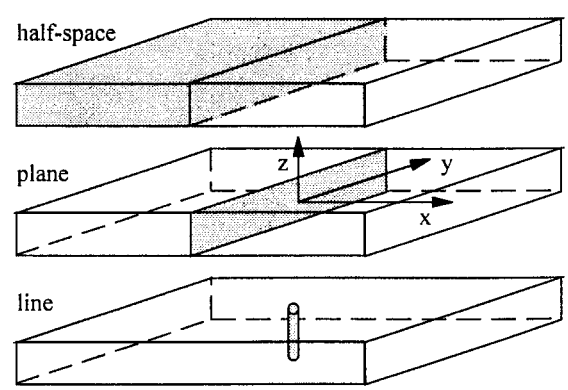

Figure 2. Schematic of geometries for half-space, plane and line kernels. Shaded portions of each diagram indicate the geometry of the electron source; geometry of the electron source is the same as that of the primary dose.

The dose distribution near a single linear absorber edge reduces to a simple result for the special case in which the photon energies (typically 2 to 15 keV for DXRL) are much larger than the K-shell binding energies of the PMMA constituents (13.6, 284.2 and 543.1 eV for hydrogen,

carbon and oxygen). Since fluorescence yields for the constituents of PMMA are all very small (<0.0083), each absorbed photon produces one photoelectron and nearly one Auger electron. Binding energies are unimportant when photon energies are large, however, so the initial energy of the photoelectron is nearly the same as that of the absorbed primary photon and the relatively low-energy Auger electron may be neglected. Further, vertical variation of the primary dose is always very small over the length scale of electron motion. Under these conditions, electrons redistribute the primary dose near an isolated absorber edge according to

$$D(x,z) = \sum_i D_i(z)\Gamma_3(\xi_i) + D_i^*(z)\Gamma_3(-\xi_i) \tag{1}$$

where $D(x,z)$ is the local total dose at a lateral position x and vertical position z, $D_i(z)$ is the local absorbed primary dose in the bright region over some interval of photon energies $E_i \pm \delta E_i$ and $D_i^*(z)$ is the primary dose under the absorber. The function Γ_3 is the half-space kernel describing electron redistribution of the bright and shadow-region primary doses. It is given by

$$\Gamma_3(\xi_i \geq 0) = \frac{1}{2}e^{-f_i} \qquad \Gamma_3(\xi_i < 0) = 1 - \frac{1}{2}e^{-f_i} \tag{2a}$$

$$f_i = 3.34|\xi_i| + 5.50|\xi_i|^{3.84} \qquad \xi_i = \frac{x - x'}{\gamma_i} \tag{2b}$$

where x' is the absorber edge location, and γ_i is the electron range in PMMA for an initial energy E_i. This electron range is obtained using the continuous slowing down approximation (CSDA). It is well approximated by

$$\gamma_i = \frac{1}{\rho}\left[\left(\frac{E_i}{7.09}\right)^{7.5} + \left(\frac{E_i}{5.95}\right)^{9.1}\right]^{0.2} \tag{3}$$

where γ_i is in micrometers, $\rho = 1.19$ g/cm^3 is the density of PMMA, and E_i is the initial electron energy in keV. This approximation was obtained by fitting numerical calculations of the CSDA range over the range of energies from 0.1 to 100 keV. The expression agrees with Murata's formulation [20,25] of the CSDA range to within 5% over these energies, based on a mean ionization energy of 70.9 eV and a zero lower bound on the electron energy.

The half-space kernel described above is applicable only to problems involving a linear absorber edge defined by bright and shadow-region widths that are both large compared to the CSDA range. For linear features not satisfying both of these restrictions, doses can be computed using a distribution of plane sources. Using this approach, and again employing the assumption of small binding energies, the total local dose and plane-source dose kernel are

$$D(x,z) = \sum_i \int D_i(x',z)\frac{\Gamma_2(\xi_i)}{\gamma_i}dx' \tag{4}$$

$$\Gamma_2(\xi_i) = \frac{1}{2}(-0.53\ln\xi_i + 1.15)e^{-f_i} \tag{5a}$$

$$f_i = 0.54\xi_i + 5.23\xi_i^{3.97} \qquad \xi_i = \frac{|x - x'|}{\gamma_i} \tag{5b}$$

Again x is the position of interest, but here x' is the plane-source location.

For still more complex geometries, doses can be computed using a distribution of line sources. Again vertical variation of the primary dose is small over the length scale of electron motion, so this approach is applicable to any feature of interest. In this case the dose and line-source kernel are

$$D(x,y,z) = \sum_i \int\int D_i(x',y',z) \frac{\Gamma_1(\xi_i)}{\gamma_i^2} dx'dy' \tag{6}$$

$$\Gamma_1(\xi_i) = \frac{1}{4}\left(\frac{0.53}{\xi_i} + 1.59\right) e^{-f_i} \tag{7a}$$

$$f_i = 0.036\xi_i + 5.01\xi_i^{4.11} \qquad \xi_i = \frac{\sqrt{(x-x')^2 + (y-y')^2}}{\gamma_i} \tag{7b}$$

Note that the spatial integrals in Eqs. 4 and 6 take into account bright and shadow regions and the spectrum of the absorbed photons through the primary doses $D_i(x')$ or $D_i(x',y')$. Also note that the Cartesian integral given in Eq 6 can be performed in radial coordinates simply by replacing the differentials $dx'dy'$ by $rdrd\theta$ and by taking $\xi_i = r/\gamma_i$.

Dose kernels for the half-space, plane and line geometries are shown in Figure 3. For all three geometries, the dose exhibits something of a plateau out to about ξ = 0.6, but then falls very quickly for still larger values. Doses beyond ξ = 1 are always negligible for the LIGA process, so the spatial integrals in Eqs 4 and 6 need never be extended to larger values. For this reason, integration of Eq 6 in radial coordinates is often beneficial since the limits of integration in the radial direction are always just r = 0 to γ_i.

Vertical profiles of bright and shadow-region primary doses are computed using LEX-D, a one-dimensional multi-wavelength model describing the spectrum of the synchrotron, x-ray transmission through any beam filters, transmission through the mask, and transmission and absorption in the PMMA resist [9]. The electron dose distributions, as presented here, are also calculated using this code.

Figure 4 shows a comparison between doses computed using LEX-D with the half-space kernel (curves) and the results of a Monte Carlo calculation (symbols) for an exposure performed at DCI [5]. The two results agree within about 15% for all spatial positions within the resist. One interesting aspect of Figure 4 is that the doses well under the absorber are insensitive to the vertical position, despite large vertical variation of doses in the bright-region. This is because the mean energy of the absorbed photons is lower at the top than it is near the bottom. As a result, the top-surface dose falls more rapidly with increasing distance under the absorber.

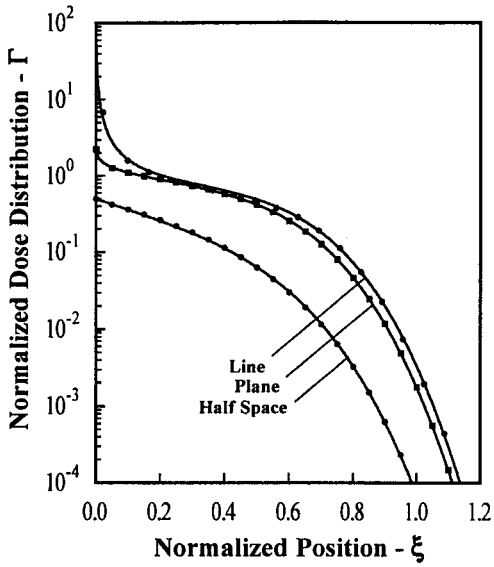

Figure 3. Dose kernels for line, plane and half-space sources. Analytical approximations (curves) are obtained by fitting the numerical results (symbols). Numerical results are based on a line source.

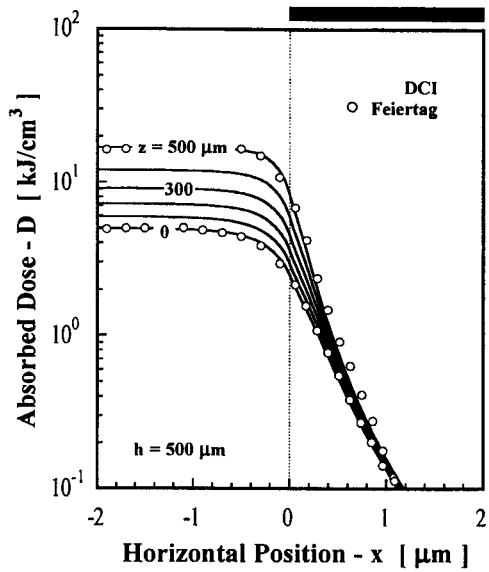

Figure 4. Dose distributions computed by analytical model (curves) and Monte Carlo method (symbols). Heavy bar above the frame indicates position of the mask absorber.

Dissolution rates, *ds/dt*, during development are governed by both reaction kinetics and the transport of PMMA fragments away from the dissolution surface. These two phenomena, acting in series, can be expressed as [26]

$$\frac{ds}{dt} = (1-c^*)\,U_0 \qquad \text{where} \qquad c^* = \frac{U_0(h-z)}{U_0(h-z_0)+\mathrm{Sh}\,\widehat{D}} \tag{8}$$

where c^* is the PMMA fragment volume fraction at the dissolution surface, h is the resist thickness, h-z is the vertical position measured from the resist top, h-z_0 is the instantaneous feature depth, U_0 is the kinetic-limited development rate at a given dose and temperature, $\widehat{D}$ is the fragment diffusivity at some given molecular weight, and Sh is the Sherwood number describing PMMA fragment transport.

The Sherwood number, based on the instantaneous feature depth, represents the ratio of the overall rate of PMMA fragment transport to the transport rate due to diffusion alone for the same vertical difference in fragment concentration. It's value in general depends on the magnitude of both forced and natural convection within a feature cavity [26,27], as well the acoustic intensity if sonic agitation is used [28]. For very large features, the Sherwood number is infinite; for very small features, it is unity.

Kinetic-limited development rates depend on the development temperature and local total dose. This is expressed in the form

$$U_0 = \alpha\left(\frac{m_\infty}{m}\right)^{\beta} e^{-\frac{E_R}{R}\left(\frac{1}{T}-\frac{1}{T_0}\right)} + \kappa\left(\frac{m_\infty}{m}\right)^{\lambda} e^{-\frac{E_D}{R}\left(\frac{1}{T}-\frac{1}{T_0}\right)} \tag{9}$$

where T_0 = 294 K (21 C) is a reference temperature and R = 8.31 J/mol-K is the ideal gas constant. The model thus contains six parameters, as well as the exposed molecular weight, m, and limiting molecular weight, m_∞, representing the smallest attainable fragment size.

The exposed molecular weight is determined by the absorbed dose, D, and initial molecular weight, m_0, according to [29]

$$\frac{m_\infty}{m} = 1 - \left[1 - \frac{m_\infty}{m_0}\right] e^{-BD} \tag{10}$$

where m_∞ = 2000 g/mol and B = 0.097 cm^3/kJ. These values of B and m_∞ were obtained by fitting measured molecular weights for doses in the range of 0.1 to 8 kJ/cm^3 and an initial molecular weight of ~2 to 4 Mg/mol [30].

Values for the six parameters were obtained by fitting measured development rates using GG developer and linear PMMA for several initial molecular weights (~2 and 4 Mg/mol) and temperatures of 21, 25 and 37 C. The results are α = 0.0041 μm/s (0.24 μm/min), β = 2.44, and E_R = 231 kJ/mol; κ = 4.01 μm/s (240 μm/min), λ = 5.05 and E_D = 142 kJ/mol [30].

Development rates given by this model are insensitive to the PMMA initial molecular weight so long as it is above about 1 Mg/mol and the dose is larger than 0.1 kJ/cm^3. Results based on this model are thus applicable to all PMMA commonly used for DXRL, with the exception of cross-linked material. Development rates for cross-linked PMMA are very significantly lower than those for the linear material at low doses [11]. This behavior can be described by changing just two of the parameters in Eq 9. The two new values for cross-linked PMMA are α = 0.00029 μm/s (0.017 μm/min) and λ = 5.36.

To compute the development history for a given feature, the distribution of the total dose is first computed for specified exposure conditions. Evolution of the feature through the development process is then calculated using a front-tracking algorithm. The front location at the start of development is specified as coincident with the top surface of the resist or, for two-dimensional sidewall features, coincident with the absorber edge. At many points along the dissolution front, the local development rate is then calculated using the local total dose and local fragment concentration. These points are then advanced in a direction orthogonal to the local front and at the speed of the local development rate. By integrating this motion in time, the evolution of the feature geometry is computed over the course of the development period.

A typical development history is presented in Figure 5 for an exposure performed at ALS operating at 1.9 GeV (bending magnet, E_c = 3.16 keV). The beam is filtered by 254 μm of beryllium, 5.6 μm of aluminum, 129 mm of air, and a 100 μm silicon mask membrane. Bottom and top doses are 3.2 and 7.5 kJ/cm^3, and the gold absorber thickness is 25 μm. The dark curves indicate the computed dissolution front at five-hour increments; gray curves indicate contours of the total dose computed using the half-space kernel. Note that development proceeds quickly at first owing to the large dose near the top surface. The dissolution front likewise advances into the masked region at a high initial rate, but slows abruptly after a short period due to rapid decay of the dose with increasing distance under the absorber. Similar behavior, though less pronounced, is seen at each elevation through the PMMA thickness. The final result is a fairly

uniform sidewall offset of about 1 μm from the absorber edge and a mean sidewall slope of only 0.25 μm/mm.

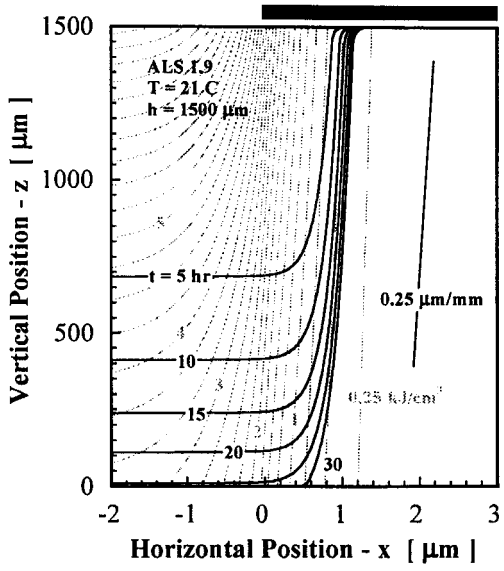

Figure 5. Development history for a 1500 μm PMMA resist. Lateral development is rapid at first, but slows at later times. Top-surface sidewall offset reaches about 1.1 μm after 25 hours of development.

Top-Surface Sidewall Offset

Based on multiple calculations like those shown in Figure 5, we find that sidewall offsets exhibit a minimum for a bottom dose between 2 and 4 kJ/cm^3, depending on the PMMA thickness and development temperature. The magnitude of this minimum increases significantly with increasing temperature above 25 C, but is reasonably insensitive to temperature between 15 and 25 C. In addition, computed sidewall offsets decrease continuously with increasing top-to-bottom dose ratio, *i.e.* a softer x-ray spectrum, but are fairly insensitive to dose ratio at values above three. Thus the optimum conditions producing minimum sidewall errors are a bottom dose of about 3 kJ/cm^3, a dose ratio of three or greater, and a development temperature of about 25 C or less. Dose ratios much above three are not usually acceptable because the PMMA will bubble or melt during exposure at top-surface doses of 10 to 20 kJ/cm^3, depending of the dose rate and exposure-induced rise in the resist temperature. In light of this, the optimum conditions are taken as a bottom dose of 3.2 kJ/cm^3, a dose ratio of three and a development temperature of 21 C.* Development times for these conditions are fairly large, but exceed the times for very large doses and high development temperatures by only a factor of three for small feature sizes.

Computed top-surface sidewall offsets based on these optimum conditions are shown in Figure 6 as a function of the resist thickness, *h*, for exposures performed at various synchrotrons. These are the offsets just as the dissolution front reaches the bottom of the resist and so correspond to the minimum possible development time. Excess development beyond this time will increase sidewall offsets at least slightly above these minimum values.

* These optimum conditions are essentially the same as those determined experimentally by Dr. F. J. Pantenburg and have been used for several years at the Institut fur Mikrostrukturtechnik, Forschungszentrum Karlsruhe.

For each resist thickness and each synchrotron, the x-ray beam is filtered only by 300 μm of beryllium and sufficient aluminum to give a top-surface dose no more than 9.6 kJ/cm^3. The bottom-surface dose is always 3.2 kJ/cm^3, and the mask absorber thickness is sufficient such that primary shadow-region doses are negligible (<10 J/cm^3). Doses due to fluorescence, diffraction and scattering are presumed to be negligible as well. Results are presented for both small (dashed) and large (solid) features. A small feature is defined here as a negative feature of width or size, w, such that $w/h \ll 1$; a large feature is defined as $w/h > 5$. These bounds yield Sh ~ 1 and Sh ~ ∞ in Eq 8, corresponding to transport-limited and kinetic-limited development rates [26]. The doses used in these calculations are based on the half-space kernel, so the results for small features apply only to cases in which the absorber width and the feature size are both large enough that doses far from the absorber edge are equal to the primary doses.

As shown in Figure 6, top-surface sidewall offsets increase strongly with resist thickness for both large and small features, and offsets are always somewhat larger for small features owing to their much longer development times [26]. The effect of feature size is fairly small, however, indicating again that sidewall offsets are reasonably insensitive to the development time. This is consistent with the sample calculation of Figure 5: sidewall dissolution is very rapid at first, but slows dramatically at later times. The symbols (Ehrfeld, Feiertag) represent measured top-surface offsets of ~0.32 μm for a thickness of 300 μm and 0.4 to 0.5 μm for a resist thickness of 500 μm [31,5]. This data is discussed in the later section on cross-linked PMMA.

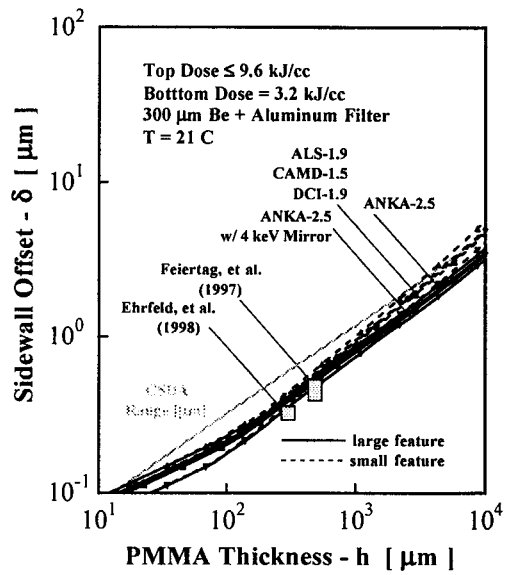

Figure 6. Minimum top-surface sidewall offset under optimum conditions increases with increasing resist thickness, but is relatively insensitive to feature size and to the synchrotron spectrum.

Figure 6 also shows that the sidewall offset is nearly independent of the x-ray source when the optimum conditions are employed. This is because each source is filtered to yield the same dose ratio, so the resist top-surface spectrum must be similar for each source at a given resist thickness. The source, however, is extremely important from a practical perspective in that it strongly influences the exposure time. The exposure time for a 1 mm resist thickness is only about 50 minutes for ANKA operating at 2.5 GeV with a mean current of 100 mA and a scan length of 50 mm. With addition of the 4 keV single mirror, this exposure time increases to more

than one month! Despite this huge disparity in exposure times, sidewall offsets for these two cases are nearly the same for any resist thickness above 200 μm.

For a resist thickness greater than 100 μm, the results in Figure 6 are fairly well described by

$$\delta \approx 0.012 h^{0.61} \quad \text{for} \quad w/h >> 1 \tag{11a}$$

$$\delta \approx 0.009 h^{0.68} \quad \text{for} \quad w/h << 1 \tag{11b}$$

for large and small features, respectively. Here δ and h are in micrometers. These relations give a reasonable approximation to the smallest sidewall offset attainable by LIGA x-ray lithography. Offsets may be reduced very slightly from these values by increasing the dose ratio or reducing the development temperature. Increasing or decreasing the bottom-surface dose from 3.2 kJ/cm^3 will not significantly reduce sidewall offset.

This dependence of the offset on resist thickness arises primarily from the increased photon energies required for exposing thicker resists without producing excessive top-surface doses. The x-ray cross-section of PMMA decreases inversely with about the cube of the photon energy, so the effective or average photon energy must increase with thickness to about the 1/3 power for a fixed dose ratio. Further, the electron CSDA range increases with initial energy to the power ~9/5 at the energies of interest. As result, the effective CSDA range for a fixed dose ratio increases with thickness to the power ~3/5 since the initial photoelectron energy is roughly the same as the photon energy. The lateral range of the shadow-region dose thus increases with thickness to the power ~0.6, and this range largely determines sidewall offset.

This is illustrated by the gray curve shown in Figure 6 labeled as the CSDA range. This is the CSDA range given by Eq 3 based on an electron energy, E, equal to the mono-energetic photon energy yielding a dose ratio of three for a given resist thickness. We see that sidewall offsets are roughly proportional to this CSDA range when the dose, dose ratio and development temperature are fixed and the resist is developed just to completion. However, the constant of proportionality depends on both the exposure and development conditions. For a bottom dose of 3.2 kJ/cm^3, a dose ratio of three and development at 21 C, the sidewall offset for large features is about 65% of this CSDA range. More generally, the constant of proportionality between the offset and CSDA electron range decreases with the about the fourth-root of the log of the dose ratio. The dependence of sidewall offset on the dose ratio is thus very weak for dose ratios between 2 and 5. In contrast, offsets are strongly affected by the development temperature and increase nearly 40%, to about 90% of this CSDA range, for development at 35 C.

Such a correlation between the sidewall offset for large features and the CSDA range implies that the top-surface sidewall develops laterally to some terminal dose that is independent of the thickness provided the bottom dose, dose ratio and development temperature are all fixed and the resist is developed just to completion. The computed terminal dose at the offset sidewall position in fact falls slightly with increasing resist thickness because the development time under these conditions grows about linearly with thickness, while the lateral extent of the dose distribution grows with thickness to about the 3/5 power. Computed terminal doses for large features and the conditions of Figure 6 range from about 0.57 kJ/cm^3 at a 100 μm resist thickness to about 0.42 kJ/cm^3 at a thickness of 1 mm. At a 5 mm thickness, this dose is about 0.33 kJ/cm^3. Terminal doses increase roughly in proportion to the bottom dose if the dose ratio

is fixed at three because sidewall offsets are insensitive to dose for bottom doses between 2 and 5 kJ/cm^3.

Offsets for small features vary more strongly with thickness than does the CSDA range. This is due to the very long development times for negative features of high aspect ratio. These times grow with the square of the thickness and far exceed those for large features of low aspect ratio when the resist thickness is more than a few hundred micrometers [26]. As a result, terminal doses at the sidewall position at the end of development also fall more significantly with increasing thickness. Computed terminal doses for small features range from about 0.55 kJ/cm^3 at a 100 μm resist thickness to about 0.30 kJ/cm^3 at a thickness of 1 mm. The terminal sidewall dose for a 5 mm thickness is just 0.14 kJ/cm^3.

Sidewall Slope

Like sidewall offsets, computed sidewall slopes generally increase with increasing development temperature and reduced dose ratio, and this temperature dependence is especially pronounced for bottom-surface doses above 4 kJ/cm^3. In contrast, however, the slopes may either increase or decrease as the bottom dose is varied for a fixed dose ratio. They tend to increase at lower doses for dose ratios below three, but decrease for ratios above three. For a dose ratio of three, the computed sidewall slope is nearly independent of the bottom-surface dose for values between 2 and 6 kJ/cm^3. The optimum conditions for sidewall offset thus also provide roughly optimum conditions for minimum sidewall slope.

Figure 7 shows the computed sidewall slope midway between the top and bottom surfaces under these optimum conditions. In contrast to offsets, the minimum mid-height slope just at the end of full development decreases with increasing PMMA thickness. Computed slopes vary from about 0.98 μm/mm for a thickness of 100 μm to 0.32 μm/mm for a 1 mm thickness. For a thickness greater than 100 μm, these results are well approximated by

$$S \approx 7.6h^{-0.46} \tag{12}$$

where the thickness h is in micrometers and the slope S is expressed in the units μm/mm. Consistent with Figure 5, slopes near the resist top are smaller than those at mid-height; those near the bottom are larger. Comparing this result to Eq 11 shows that the sidewall slope is significantly less than the top-surface sidewall offset divided by the resist thickness, indicating again that the sidewall profile is not linear between the top and bottom of the resist. For a thickness greater than about 100 μm, the mid-height slope is roughly 30% of this ratio. This is also consistent with Figure 5.

The results of Figure 7 indicate that sidewall slopes, like sidewall offsets, are insensitive to the source spectrum and feature size. This insensitivity to feature size is somewhat surprising since development times differ significantly for small and large features when the resist thickness is large. At a 1 mm thickness, development times range from about 15 hours for large features to roughly 42 hours when the feature size is very small. For a 10 mm resist, these times vary from about 130 hours to nearly 4 months. Nevertheless, the sidewall slopes for small and large features at a 10 mm thickness differ by less than 30% for a given source.

The reason for this unexpected behavior is that small features of high aspect ratio yield long development times due to high concentrations of PMMA fragments at the dissolution front. These high concentrations also reduce lateral development rates at the mid-height of the feature (once the development front has passed) and so longer development times due to PMMA fragment transport do not significantly affect sidewall slopes. In contrast, over-development can significantly reduce sidewall slopes. Over-development by a factor of two in time reduces mid-height slopes by about 20%; a factor of three reduces slopes by about 30%. Equation 12 thus represents the minimum possible slope for development just to completion, but smaller slopes can be obtained if the resist is substantially over-developed. This will, of course, lead to slightly increased sidewall offsets.

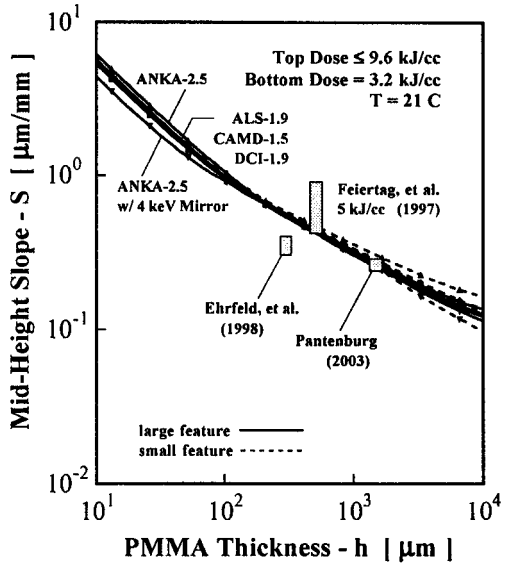

Figure 7. Sidewall slope midway between the resist top and bottom surfaces. Values shown are just at the end of full feature development. Symbols represent measured slopes [6,31,32].

Figure 7 additionally shows symbols representing measured sidewall slopes. These are mid-height slopes discerned from the sidewall profiles reported by Ehrfeld and Schmidt for a 300 μm resist thickness [31], by Feiertag *et al.* for a 500 μm thickness on a carbon substrate [5] and by Pantenburg for a thickness of 1500 μm [32]. The Ehrfeld result and that of Feiertag employed cross-linked PMMA, while the result of Pantenburg used a linear form of the resist. Bottom doses for the first and second of these were 5 kJ/cm^3; dose ratios were about 2.9 and 3.3, respectively. The bottom dose for the third was 3.2 kJ/cm^3, and the dose ratio was about 2.1. Exposure conditions for these three results were thus roughly optimal.

These measured slopes at near-optimum conditions lie fairly close to the predicted minimum values, though the data do show considerable variation. In particular, the result of Ehrfeld and Schmidt (~0.35 μm/mm) is roughly 35% lower than the predicted minimum value at a resist thickness of 300 μm (~0.55 μm/mm). This small sidewall slope likely results from the effects of fluorescence from the titanium substrate used in their experiment and, perhaps, slight over-development. For exposure at BESSY under their conditions, the computed mid-height sidewall slope for cross-linked PMMA is 0.61 μm/mm just at the end of development at 37 C; this drops to about 0.41 μm/mm when the fluorescence dose is also considered. This is because fluorescence from the substrate produces total shadow-region doses that increase with depth in

the vicinity of the substrate, resulting in negative sidewall slopes close to the substrate and a slightly reduced positive slope at mid height. If, in addition, the resist is over-developed by just 10 minutes at 37 C, then the computed mid-height slope drops to 0.24 μm/mm; an extra 20 minutes reduces the slope to just 0.15 μm/mm. However, over-development by 20 minutes still yields a slope of 0.43 μm/mm at this temperature when fluorescence radiation is neglected. This wide range of computed slopes thus bounds the measured value of about 0.35 μm/mm, but also demonstrates the potential of substrate fluorescence in reducing sidewall slopes. Such fluorescence may also contribute to the low mean slopes of about 0.25 μm/mm reported much earlier by Munchmeyer and Ehrfeld for a 400 μm resist thickness [2]. This speculation cannot be confirmed, however, as their exposure conditions, development time and substrate material were not reported.

Minimum Feature Size

The minimum sizes of positive and negative features that can be produced by DXRL are determined by the dose distribution surrounding the feature and the required development time. As the feature width approaches the electron CSDA range, electron dose distributions from the bright regions bounding a positive feature begin to overlap, and the minimum shadow-region dose under the absorber increases. Similarly, the maximum bright-region dose decreases for negative features as the feature becomes very small. The result for both positive and negative features is reduced dose contrast, leading to large discrepancies between the mask pattern and the PMMA structure once the resist is fully developed. Moreover, some small features cannot be produced at all at a given thickness since the top of the structure will be dissolved completely during the required development time.

Figure 8 shows dose profiles near an isolated linear absorber defining a positive linear feature in the developed resist. A bar at the top of the figure indicates the absorber position. The horizontal axis is the lateral position scaled by the width of the mask absorber; the vertical axis is the local dose at the mid-height, z = 250 μm, of a 500 μm resist. These results, for varied absorber widths, were computed using Eq 4 and the plane-source dose kernel given in Eq 5 based on the spectrum of ALS operating at 1.9 GeV. The beam is filtered only by 300 μm of beryllium and 19.1 μm of aluminum to give top and bottom doses of 9.6 and 3.2 kJ/cm^3, respectively; absorber thickness is 25 μm, and the mid-height dose far from the feature is 5.0 kJ/cm^3.

The results in Figure 8 show that the minimum dose under the absorber begins to increase significantly for mask absorber widths, w_m, below about 10 μm. For a 2 μm width, the minimum dose under the absorber increases to about 0.19 kJ/cm^3, corresponding to a maximum dose contrast of about 25. This minimum dose increases to about 3.5 kJ/cm^3 as the feature width is reduced to 0.2 μm, and the dose contrast drops to just over unity. The effect of these geometry-dependent doses on developed feature dimensions is illustrated in Figure 9. The values shown, for various absorber widths, are the feature widths at the top of the structure just at the end of development. Here the development time depends on the resist thickness, but is independent of the feature size since the exposed areas surrounding the feature are very large. These results thus do not account for the possibility that other features on the same resist may require longer

development times. Top and bottom doses for each feature width and each resist thickness are 9.6 and 3.2 kJ/cm^3, respectively. As before, this dose ratio is maintained using 300 μm of beryllium and an aluminum filter of appropriate thickness.

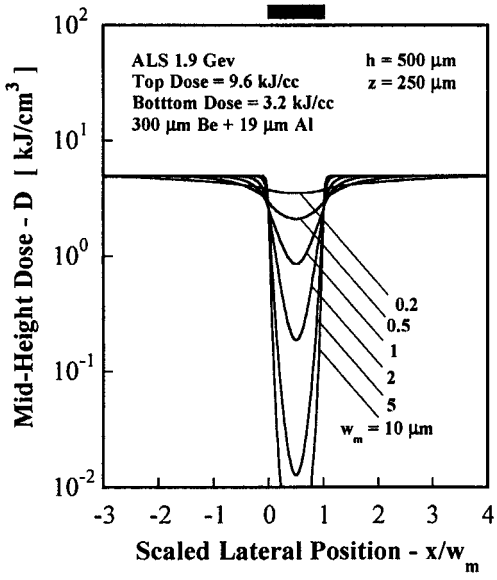

Figure 8. Dose profiles near a mask absorber defining a positive feature in the resist. Minimum shadow-region doses under the absorber increase as the feature width becomes small.

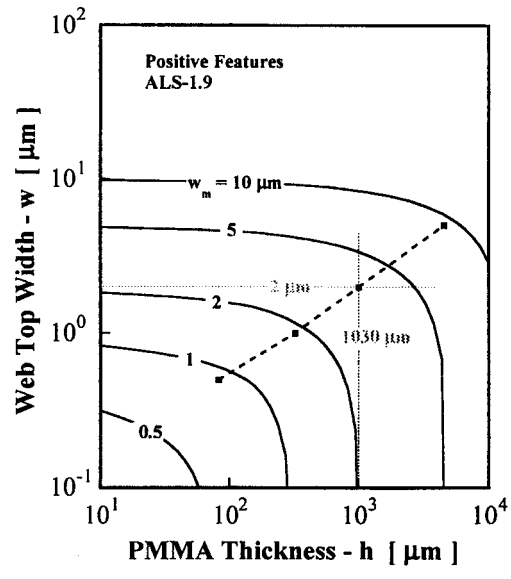

Figure 9. Top surface widths of developed structures. Points and dashed curve show minimum absorber width for which the top width of the developed structure is just above zero.

Figure 9 shows that the top width of the developed feature is comparable to the absorber width when the feature size is large or the resist thickness is sufficiently small. For example, we see that the developed feature width for a 2 μm absorber width will be about 1.8 μm for a resist thickness of 10 μm. This dimension falls to about 1.6 μm for a 100 μm thickness. We also see that the developed feature width falls rather abruptly to zero at some value of the resist thickness that depends only on the width of the absorber. For example, the 2 μm absorber width produces a zero width at the structure top for a resist thickness of about 1 mm, as indicated by the gray lines. These critical widths are shown for all thicknesses by the points and dashed curve. Absorber widths smaller than these values will produce knife-edge structures following development, and the height of these structures will be less than the original resist thickness. This dashed curve thus represents the minimum possible size of a positive feature producible by LIGA at a given resist thickness. For thicknesses above 100 μm, these values are fairly well approximated by

$$w_m \approx 0.029 h^{0.61} \qquad \text{or} \qquad A_{\max} \approx 34 h^{0.39} \tag{13}$$

where the absorber width w_m and the resist thickness h are both in micrometers. Dividing the minimum feature width by the resist thickness yields the maximum possible aspect ratio, $A_{\max}$; this is also given in Eq 13. The minimum possible sizes for positive linear structures are thus about 0.5 and 2.0 μm for thicknesses of 100 μm and 1 mm, respectively. The corresponding maximum possible aspect ratios for these thicknesses are about 200 and 500.

The minimum feature size given in Eq 13 is not just twice the offset for large features as described in Eq 11, but is instead somewhat larger. This is because Eq 11 is applicable only to cases in which the absorber width is large compared to the electron range. Equation 13, on the other hand, takes into account the overlap of dose fields under the absorber due to electrons emitted from bright regions on both sides of the feature.

Small positive features are relatively easy to produce because doses in exposed regions of the PMMA are not much affected by the feature size. In contrast, maximum bright-region doses for small negative features fall as the feature becomes small. This increases development times and so increases the extent of sidewall dissolution. Countering this by increasing the primary dose is not usually an option because doses in any large negative features on the same resist will then be excessive. Small negative features are additionally subject to diffusion-limited development rates, and this further increases development times and sidewall dissolution [26].

Figure 10 illustrates the effect of aperture size, w_o, on the dose distribution produced by a linear opening in the mask absorber intended to produce a long trench in the developed resist. These doses were again computed using the plane-source kernel. For a resist thickness of 500 μm, the maximum bright-region dose begins to decay for aperture widths below 5 μm, and that this dose drops rapidly for still smaller widths. The lateral span of the dose distribution also significantly exceeds the aperture width when the aperture is very small. This behavior is completely analogous to that discussed earlier for positive features. Here, however, the feature is defined by an opening in the mask absorber, so doses within the feature decrease as the feature width becomes small due to electrons escaping from the bright region into surrounding areas under the absorber.

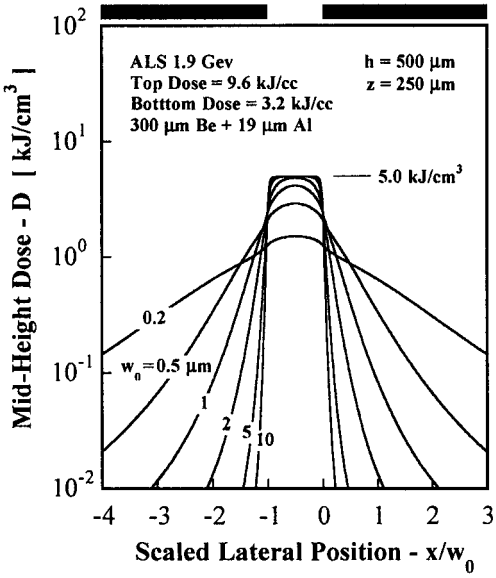

Figure 10. Dose profiles for a trench-like negative feature. Maximum open-area doses fall as the feature width becomes small, and shadow-region doses extend to a larger range relative to mask aperture size w_0.

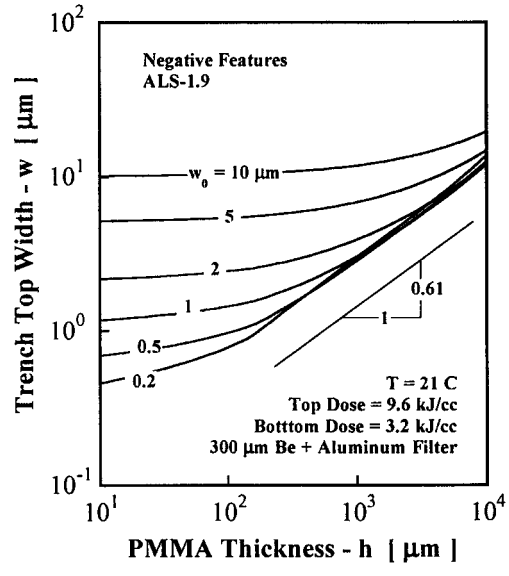

Figure 11. Feature width at resist top surface for negative features. Width is independent of mask aperture when resist thickness is large. Minimum feature size is about 1.4 μm for a 300 μm thickness.

Top-surface widths of developed trench-like features are shown in Figure 11. Here, the smallest possible feature width increases with increasing resist thickness and is roughly three times the sidewall offset given in Figure 6. Further, the width of the developed trench is nearly independent of the aperture width when the aperture is smaller than the sidewall offset. Thus the smallest possible negative feature size is about 0.7 μm for a resist thickness of 100 μm; this increases to about 3 μm for a thickness of 1 mm. Note in Figure 11 that small apertures may give developed feature widths exceeding those for larger apertures when the resist is very thick. The envelope of these curves thus determines the minimum producible size.

Based on the results in Figure 11, the minimum width for negative trench-like features, and the corresponding maximum aspect ratio, are reasonably well approximated by

$$w_o \approx 0.042 h^{0.61} \quad \text{or} \quad A_{\max} \approx 24 h^{0.39} \tag{14}$$

Again the width and resist thickness are both in micrometers. The minimum size for negative features is thus about 50% larger than that for positive features at the same resist thickness.

Fine Features on Larger Structures

Sidewall tolerances and minimum feature size are readily defined and quantified for simple isolated features such as lines and trenches. This is not the case for fine features patterned on the sidewalls of larger structures. Such features assume a wide variety of geometries and, at a minimum, the geometries tend to be complex due to the fact that the sidewall edge is a part of the structure. A somewhat empirical approach is therefore useful in characterizing producible feature dimensions. Here, the final dimensions of several prototypical features are computed, and the results are used to draw general conclusions based on the sidewall offsets and minimum feature sizes already calculated for isolated structures.

Figure 12 illustrates several features patterned in this manner. The upper panel shows contours of the dose looking down on the features, orthogonal to the plane of the resist. These doses were computed for a resist thickness of 500 μm and the geometry shown using the line-source kernel given in Eq 7. The source is ALS operating at 1.9 GeV and the beam is filtered by 300 μm of beryllium and 19.1 μm of aluminum to obtain bottom and top primary doses of 3.2 and 9.6 kJ/cm^3. The development time under these conditions is about 8 hours for a development temperature of 21 C. The width of each feature is 1.2 μm at the base along the sidewall edge, and the heights of the square, peak and dome structures are 1.2, 2.0 and 1.4 μm, respectively.

A history of the lateral development near the resist top surface is shown in the lower panel of Figure 12. As usual, offsets from the absorber edge grow rapidly at first and then slow dramatically as the dissolution front advances into low-dose regions. Following complete development, these structures do not remotely resemble the mask pattern, and the structure heights are reduced to just 0.7, 0.5 and 0.7 μm for the square, peak and dome. In contrast, the same structures patterned as indentations into the sidewall retain some semblance of the absorber pattern. This is shown in Figure 13. Here the developed structure heights are 1.1, 1.5 and 1.3 μm for the square, peak and dome.

Despite obvious differences between the development front profiles of Figures 12 and 13, the two results share one common characteristic: to first approximation, the developed structures in each figure resemble the absorber pattern uniformly offset by about 0.53 μm in a direction normal to the feature boundary. This is the offset given by Eq 11a for a resist thickness of 500 μm. The consequence of this offset, however, is very different in the two cases. For the protrusions, structure geometry is largely destroyed. This is because the width of the absorber defining these structures is just less than the minimum size for a positive feature, as given by Eq 13. The developed structures would thus recede to the vicinity of the sidewall edge (at the top surface) regardless of their height. In contrast, the indented features simply grow larger in the direction parallel to the sidewall edge while preserving, to some extent, dimensions in the normal direction.

One notable exception to such uniform offset is at corners of the absorber pattern. Doses at the vertex of an inside corner are about half of those and the sidewall edge, while doses at an outside corner are about 50% larger. Offsets near an outer corner are thus larger than the sidewall offset; those near an inner corner are smaller. As a result, developed structures exhibit inside radii that are larger than outside radii.

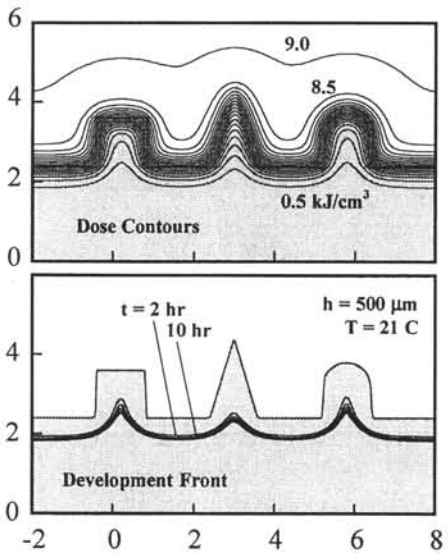

Figure 12. Dose distribution and development history for fine features protruding from a larger structure. Developed features (lines) do not resemble mask pattern (gray). Dimensions are in micrometers.

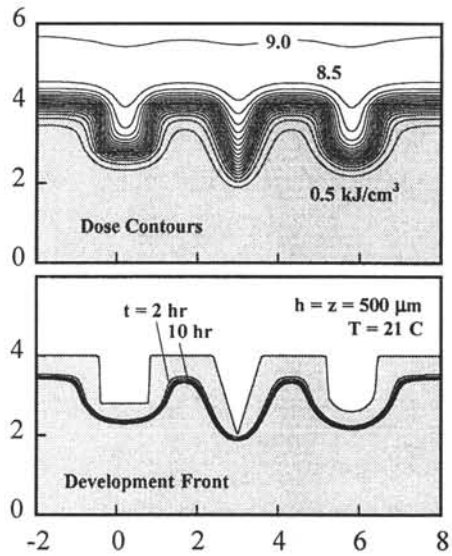

Figure 13. Doses and development history for indented features. Mask pattern is the same as shown Figure 12 but tone is reversed. Developed features vaguely replicate mask pattern.

To help quantify this phenomenon, consider the problem of a single isolated step as shown in Figure 14. The step face is orthogonal to the sidewall edge, the step run is much longer than the step height, and the step height is large enough such that dose distributions surrounding the inner and outer corners do not overlap significantly. Figure 14 shows profiles of the top-surface development front for a 500 μm and a 1500 μm thickness. Top and bottom doses are 9.6 and 3.2 kJ/cm^3 in each case, and each was developed just to completion at 21 C.

We see in both panels that the minimum radius on the outer corner of the developed structure is almost a factor of three smaller than the minimum radius of the inner corner. We also see that these minimum radii scale with thickness in the manner of the sidewall offset for large features. That is,

$$r_i \approx 0.019 h^{0.61} \qquad \text{and} \qquad r_o \approx 0.0049 h^{0.61} \tag{14}$$

for 90-degree corners in the absorber pattern. The minimum inner radius is thus about twice the offset given by Eq 11a, while the minimum outer radius is about half this value. These expressions give r_i = 0.84 μm and r_o = 0.22 μm for the 500 μm resist thickness used in Figure 14. For a thickness of 100 μm, the minimum radii are 0.32 and 0.08 μm; for h = 1 mm they are 1.28 and 0.33 μm, respectively. These results apply to all cases in which the developed region surrounding the structure is sufficiently large that its aspect ratio is small. They therefore apply also to the outside corners of isolated positive features. However, the radii of inside corners of small isolated negative features may differ somewhat due to the much longer development times.

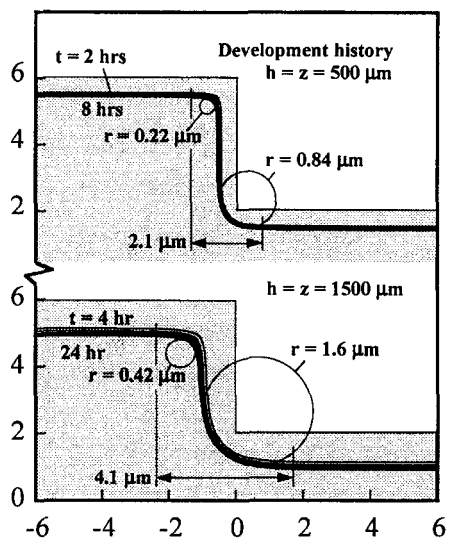

Figure 14. Development history for a step. Minimum radii increase with increasing thickness, and radii of inner and outer corners differ significantly. Step height is preserved, but the step profile is blurred. Dimensions are in micrometers.

Note in Figure 14 that some rounding of each corner extends well beyond the range of the minimum radius. On the outer corner, this affected region is a little more than three times the outer radius as measured from the step face of the developed structure; for the inner corner the affected region is about 1.5 times the radius. The step is thus blurred over a region significantly larger than the sum of the minimum inner and outer radii, and the overall step width is approximately given by

$$w_{\text{step}} \approx 0.047 h^{0.61} \tag{15}$$

where the width and thickness are in micrometers. This result is in good agreement with a step profile previously measured [33]. For a resist thickness of 850 μm, linear PMMA and development at 21 C, the measured full step width is about 3.1 μm in a direction parallel to the run of the step. In comparison, Eq 15 yields 2.9 μm for this thickness.

Cross-linked PMMA

All of the results presented so far are based on linear PMMA. These results are applicable to any molecular weight greater than about 1 Mg/mol, so long as the PMMA is not cross-linked. As mentioned before, cross-linked PMMA exhibits lower development rates, especially at low doses, and these lower rates affect sidewall tolerances and the minimum feature size. Using the same optimum conditions for the dose, dose ratio and development temperature, computed sidewall offsets for the cross-linked resist are about 80% of those for linear PMMA. Likewise, the minimum producible feature sizes and minimum radii for cross-linked PMMA are about 80% of those for the linear material. In contrast, sidewall slopes at the mid-height of the resist are essentially identical for the two resist materials. Thus, the previous discussion of sidewall slopes made no distinction between cross-linked PMMA (Ehrfeld, Feiertag) and the linear form (Pantenburg).

The measured offsets shown in Figure 6 are both results for cross-linked PMMA, and this accounts for the fact that the measured values lie slightly below the minimum offsets computed for linear PMMA. The offset measured by Ehrfeld and Schmidt [31] was about 0.32 μm for exposure at BESSY (E_c = 2.13 keV), a resist thickness of 300 μm, a bottom dose of 5 kJ/cm^3, and a dose ratio of 2.9. In comparison, Eq 11a yields a minimum offset of 0.39 μm at this thickness, and 80% of this value is 0.31 μm. Their measured offset is thus just slightly above the minimum value computed here for the cross-linked resist. Similarly, the offsets measured by Feiertag *et al.* [5] ranged from 0.4 to 0.5 μm for exposure at DCI (E_c = 3.70 keV), a resist thickness of 500 μm, a bottom dose of 5 kJ/cm^3, and a dose ratio of 3.3. In this case, Eq 11a yields a minimum offset of 0.53 μm for linear PMMA and a thickness of 500 μm, and 80% of this is 0.43 μm. Again, these measured offsets lie very close to or slightly above the expected minimum value.

This scaling is further illustrated by the dose contours and the developed sidewall position shown in Figure 15 for a stepped structure. The step height is 1.2 μm, the step run is 6 μm and the step angle on the mask pattern is 90 degrees. This geometry is a small portion of a spectrometer grating that was fabricated and measured by Achenbach, *et al.* at resist thickness of 850 μm, using a bottom-surface dose of 3.7 kJ/cm^3 and a dose ratio of about 4 [33]. The exposure was performed at ELSA (E_c = 2.48 keV). Computed sidewall offsets, near the top of the resist and far from the step, are about 0.74 μm for the linear resist, but only about 0.61 μm for the cross-linked PMMA. This is roughly consistent with the 80% guideline. The measured width of the developed step for the cross-linked resist and development at 21 C is about 2.3 μm. Again, this is consistent with 80% of the value given by Eq 15 for a resist thickness of 850 μm.

The data shown in Figure 15 (symbols) are the measurements made by Achenbach for cross-linked PMMA at a position somewhat below the top surface of the resist. Those measurements gave the step profile, but could not provide the position of the profile relative to the mask pattern. The measured profile was thus translated to align with the computed results along the run of the step. As such, the only valid comparison between the computed and measured results is the contour of the step. These agree very well, however, over the full step width.

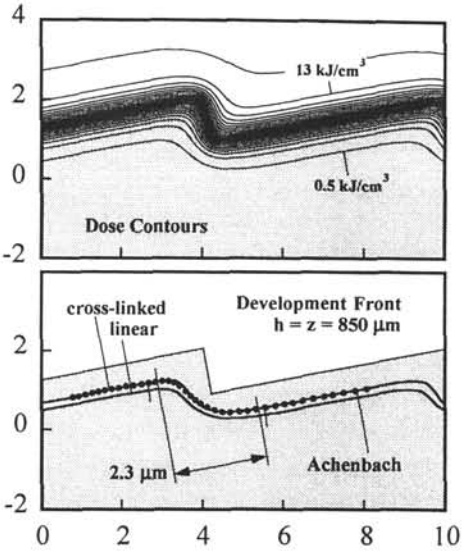

Figure 15. Dose contours and final sidewall position for a stepped structure. Computed sidewall offsets far from the step using cross-linked PMMA are about 80% of those for the linear material. Dimensions are in micrometers.

Smaller offsets for cross-linked PMMA also yield larger terminal doses at the sidewall position just at the end of development. For linear PMMA, this dose at the top surface is about 0.43 kJ/cm^3 for large features exposed and developed at optimum conditions, a resist thickness of 850 μm and a top dose of 9.6 kJ/cm^3. This increases to 0.60 kJ/cm^3 for cross-linked PMMA under the same conditions. The higher doses used by Achenbach yield computed terminal doses of 0.46 and 0.69 kJ/cm^3 for linear and cross-linked resists. Likewise, Ehrfeld and Schmidt [31] observed that the computed dose at the top-surface sidewall position was about 1 kJ/cm^3 for a cross-linked resist, a top-surface primary dose of about 14.4 kJ/cm^3 and a dose ratio of about 2.9. The terminal dose computed here for their problem is slightly lower, about 0.93 kJ/cm^3. This value is significantly larger than the terminal doses discussed above owing to the large top-surface dose and lower dose ratio.

Summary

For nearly all cases of practical interest, feature tolerances and the minimum feature size producible by LIGA x-ray lithography are fundamentally limited by the redistribution of primary doses via photoelectrons and the influence of the resulting dose distribution on resist development. This fundamental limitation of the LIGA process is investigated here using analytical and numerical methods.

Analytical dose kernels describing photoelectron doses are presented for half-space, plane and line sources. These kernels, along with primary doses computed numerically, are used to compute dose distributions for a single absorber edge, for small isolated features and for small features on larger structures. This dose field is then used to compute development histories. Sidewall offset, slope and the minimum producible feature size are obtained from the final feature geometry.

Sidewall offsets are minimized for bottom-surface doses of 2 to 4 kJ/cm^3. Offsets decrease continuously with decreased development temperature and increased dose ratio, but are fairly

insensitive to the temperature below 25 C and to the dose ratio for values above three. Sidewall slopes exhibit a more complex behavior, but again exhibit practical minima for a bottom-surface dose of about 3 kJ/cm^3, a dose ratio of about three and a development temperature less than 25 C. From these observations, general optimum conditions are taken as a bottom dose of 3.2 kJ/cm^3, a dose ratio of three and a development temperature of 21 C. These optimum conditions are insensitive to the resist thickness and insensitive to the spectrum of the synchrotron. Moreover, the developed feature geometries are insensitive to the synchrotron spectrum when the spectrum is properly filtered to produce the optimum dose ratio.

For exposure and development at these optimum conditions, sidewall offsets grow with resist thickness to the 0.61 power for isolated positive features or negative features of low aspect ratio. For small negative features of high aspect ratio, offsets grow with thickness to the power 0.68. This dependence on thickness is due mostly to the increased effective photon energy required for increased resist thickness. Minimum possible sidewall offset for linear PMMA and a resist thickness of 500 μm is about 0.53 μm for low aspect ratios; it is about 0.63 μm for negative features when the aspect ratio is high. In contrast, sidewall slopes generally decrease with increasing thickness to the power 0.46 and are relatively insensitive to feature aspect ratio. For a 500 μm thickness, the minimum sidewall slope at half-height is about 0.44 μm/mm just as development is completed. However, sidewall slopes can be reduced significantly by over-development. Fluorescence radiation from the PMMA substrate may also reduce sidewall slopes.

The minimum positive and negative feature sizes producible by LIGA DXRL also increase with thickness to the power 0.61; maximum aspect ratios thus increase with increasing thickness to the power 0.39. For positive features, this minimum size is the minimum width of an absorber structure that produces a non-zero width at the top of the developed structure. For negative features, it is that smallest width at the top of a developed feature producible by any mask aperture. The developed width of the feature is nearly independent of the mask aperture for apertures smaller than this size. Minimum producible sizes for positive and negative features are 1.3 and 1.9 μm, respectively, for a 500 mm resist thickness. Corresponding aspect ratios for these features are 380 and 270.

Minimum producible sizes of fine features on the sidewalls of larger structures once again grow with resist thickness to the power 0.61, but exhibit a pronounced dependence on tone. Sidewall protrusions having both lateral dimensions less than about five times the sidewall offset cannot be produced, while similar structures patterned as indentations retain credible semblance of the mask pattern even when the feature dimensions are comparable to the sidewall offset. Shallow step-like structures having a large dimension along the sidewall edge can be produced, subject to an offset, with accuracies in step height not limited by the photoelectron dose distribution. In such cases, dimensional errors arise only in rounding of the two corners defining the step location.

At such corners, the minimum producible radii grow with resist thickness to the power 0.61 when the aspect ratio of the surrounding developed region is low. Minimum radii for inside corners are about four times those of outside corners, and the overall step width is about twice the sum of the inner and outer radii. Typical minimum radii for a 500 μm resist thickness are

about 0.84 and 0.22 μm for inside and outside corners, respectively, based on 90-degree angle of the mask pattern. The minimum overall step width at this thickness is about 2.1 μm.

All previous results here apply to linear PMMA. Cross-linked PMMA reduces sidewall offset, minimum producible feature sizes and minimum radii by about 20%. Minimum sidewall slopes are nearly the same for the linear and cross-linked materials.

Acknowledgment

The author thanks Dr. Aili Ting for computing the line-source dose distributions employed in this study. This work was funded by Sandia's Materials Science Research Foundation. Sandia National Laboratories is operated by Sandia Corporation for the United States Department of Energy under contract DE-AC04-94AL85000.

References

1. E. W. Becker, W. Ehrfeld, P. Hagmann, A. Maner, D. Munchmeyer, "Fabrication of Microstructures with High Aspect Ratios and Great Structural Heights by Synchrotron Radiation Lithography, Galvanoforming and Plastic Moulding (LIGA Process)," *Microelectronic Eng.*, **4**, 35-56, 1986.

2. D. Munchmeyer and W. Ehrfeld, "Accuracy Limits and Potential Applications of the LIGA Technique in Integrated Optics," Proceedings of the SPIE, *Micromachining of Elements with Optical and other Submicrometer Dimensional and Surface Specification,* **803**, 72-79, 1987.

3. W. Ehrfeld, P. Bley, F. Gotz, J. Mohr, D. Muchmeyer, W. Schelb, H. J. Baving, D. Beets, "Progress in Deep-Etch Synchrotron Radiation Lithography," *J. Vac. Sci. Technol. B*, **6**, 178-182, 1988.

4. G. Feiertag, W. Ehrfeld, H. Lehr, A. Schmidt and M. Schmidt, "Accuracy of Structure Transfer in deep X-Ray Lithography," *J. Microelectronic Eng.*, **35**, 557-560, 1997.

5. G. Feiertag, W. Ehrfeld, H. Lehr, A. Schmidt and M. Schmidt, "Calculation and Experimental Determination of the Structure Transfer Accuracy in Deep X-Ray Lithography," *J. Micromech. Microeng.*, **7**, 323-331, 1998.

6. H. Zumaque, G. A. Kohring and J. Hormes, "Simulation Studies of Energy Deposition and Secondary Processes in Deep X-Ray Lithography," *J. Micromech. Microeng.*, **7**, 79-88, 1997.

7. F. J. Pantenburg and J. Mohr, "Influence of Secondary Effects on the Structure Quality in Deep X-Ray Lithographie," *Nucl. Instrum. Methods Phys. Res. B*, **97**, 551-556, 1995.

8. F. J. Pantenburg, A. Achenbach and J. Mohr, "Characterization of Defects in Very High Deep-Etch X-Ray Lithography Microstructures," *Microsyst. Technol.*, **4**, 89-93, 1998.

9. S. K. Griffiths and A. Ting, "The Influence of X-Ray Fluorescence on LIGA Sidewall Tolerances," *Microsyst. Technol.*, **8**, 120-128, 2002.

10. S. Achenbach, F. J. Pantenburg, J. Mohr, "Numerical Simulation of Thermal Distortions in Deep and Ultra-Deep X-Ray Lithography," *Microsyst. Technol.*, **9**, 220-224, 2003.

11. F. J. Pantenburg, A. Achenbach and J. Mohr, "Influence of Developer Temperature and Resist Material on the Structure Quality in Deep X-Ray Lithography," *J. Vac. Sci. Technol B.*, **16**, 3547-3551, 1998.

12. A. Schmidt, A. Clifton, W. Ehrfeld, G. Feiertag, H. Lehr and M. Schmidt, "Investigation of the Adhesive Strength of PMMA Structures on Substrates Obtained by Deep X-Ray Lithography," *J. Microelectronic. Eng.*, **30**, 215-218, 1996.

13. A. El-Kholi, K. Bade, J. Mohr, F. J. Pantenburg and X. M. Tang, "Alternate Resist Adhesion and Electroplating Layers for LIGA Process," *Microsyst. Technol.*, **6**, 161-164, 2000.

14. F. De Carlo, J. J. Song and D. C. Mancini, "Enhanced Adhesion Buffer Layer for Deep X-Ray Lithography," *J. Vac. Sci. Technol. B*, **16**, 3539-3542, 1998.

15. A. Ruzzu and B. Matthis, "Swelling of PMMA Structures in Aqueous Solutions and Room Temperature Ni-Electroforming," *Microsyst. Technol.*, **8**, 116-119, 2002.

16. G. Aigeldinger, J. T. Ceremuga and D. M. Skala, "Large Batch Dimensional Metrology Demonstrated in the Example of a LIGA Fabricated Spring," proceedings of the fifth international workshop on High Aspect Ratio Microstructure Technology (HARMST'03), Monterey, California, June 15-17, 2003.

17. S. K. Griffiths and J. A. W. Crowell, "Dimensional Errors in LIGA-Produced Metal Parts due to Thermal Expansion and Swelling of PMMA," proceedings of the fifth international workshop on High Aspect Ratio Microstructure Technology (HARMST'03), Monterey, California, June 15-17, 2003.

18. K. Murata, M. Tanaka and K. Kawata, "Theoretical Study of Energy Absorption in X-Ray Lithography with Monochromatic X-Rays," *Optik*, **84**, 163-168, 1990.

19. K. Murata, "Theoretical Studies of the Electron Scattering Effect on Developed Pattern Profiles in X-Ray Lithography," *J. Appl. Phys.*, **57**, 575-580, 1985.

20. K. Murata, M. Kotera, K. Nagami and S. Namba "Monte Carlo Modeling of the Photo and Auger Electron Production in X-Ray Lithography with Synchrotron Radiation," *IEE Trans. Electron. Devices*, **ED-32**, 1694-1703, 1985.

21. L. E. Ocola and F. Cerrina, "Parametric Modeling of Photoelectron Effects in X-Ray Lithography," *J. Vac. Sci. Technol. B*, **11**, 2839-2844, 1993.

22. M. Feldman and J. Sun, "Resolution Limits in X-Ray Lithography," *J. Vac. Sci. Technol. B*, **10**, 3173-3176, 1992.

23. H. Betz, K. Heinrich, A. Heuberger, H. Huber and H. Oertel, "Resolution Limits in X-Ray Lithography Calculated by Means of X-Ray Lithography Simulator XMAS," *J. Vac. Sci. Technol. B*, **4**, 248-252, 1986.

24. J. A. Halbleib, R. P. Kensek, G. D. Valdez, S. M. Seltzer and M. J. Berber, "ITS: The integrated TIGER Series of Electron/Photon Transport Codes – Version 3.0," *IEEE Trans. Nucl. Sci.*, **39**, 1025-1030, 1992.

25. T. S. Raho-Sahib and D. B. Wittry, "X-Ray Continuum from Thick Elemental Targets for 10-50 keV Electrons," *J. Appl. Phys.*, **45**, 5060-5068, 1974.

26. S. K. Griffiths and R. H. Nilson, "Transport Limitations on Development Times of LIGA PMMA Resists," *Microsyst. Technol.*, **8**, 335-342, 2002.

27. R. H. Nilson and S. K. Griffiths, "Natural Convection in Trenches of High Aspect Ratio," *J. Electrochem. Soc.*, **150**, C401-412, 2003.

28. S. K. Griffiths and R. H. Nilson, "Enhanced Transport by Acoustic Streaming in Deep Trench-Like Cavities," *J. Electrochem. Soc.*, **149**, 286-296, 2002.

29. E. M. Lehockey, J. D. Wice and I. Reid, "Dissolution Characteristics of Poly(Methyl Methacrylate) as an X-Ray Resist," *Can. J. Phys.*, **65**, 975-979, 1987.

30. F. J. Pantenburg, M. A. Bankert, L. A. Domeier, S. K. Griffiths and K. C. Wepfer, "Development Rates of LIGA PMMA X-Ray Resists," proceedings of the fifth international workshop on High Aspect Ratio Microstructure Technology (HARMST'03), Monterey, California, June 15-17, 2003.

31. W. Ehrfeld and A. Schmidt, "Recent Developments in Deep X-Ray Lithography," *J. Vac. Sci. Technol. B*, 16, 3526-3534, 1998.

32. F. J. Pantenburg and S. K. Griffiths, "Measurement of LIGA Resist Line-Width Deviations," proceedings of the fifth international workshop on High Aspect Ratio Microstructure Technology (HARMST'03), Monterey, California, June 15-17, 2003.

33. A. Achenbach, J. Mohr and F. J. Pantenburg, "Application of Scanning Probe Microscopy for the Determination of High Aspect Ratio Microstructures," *J. Micromech. Microeng.*, **53**, 637-640, 2000.

Distribution

R. G. Steinhoff
Honeywell Federal Manufacturing
& Technologies
PO Box 419159
Kansas City, MO 64141

M. Widmar
Honeywell Federal Manufacturing
& Technologies
PO Box 419159
Kansas City, MO 64141

L. Zawiki
Honeywell Federal Manufacturing
& Technologies
PO Box 419159
Kansas City, MO 64141

B. L. Dearth
Honeywell Federal Manufacturing
& Technologies
PO Box 419159
Kansas City, MO 64141

K. McNair
Honeywell Federal Manufacturing
& Technologies
PO Box 419159
Kansas City, MO 64141

W. Ehrfeld
Ehrfeld Mikrotechnik AG
Mikroforum Ring 1
D-55234 Wendelsheim
Germany

S. Megtert
LURE Batiment 209 D
Centre Universitaire Paris Sud
91898 Orsay cedex
France

V. Saile
Institut fur Mikrostrukturtechnik
Forschungszentrum Karlsruhe
Hermann-von-Helmholtz-Platz 1
76344 Eggenstein-Leopoldshafen
Germany

J. Mohr
Institut fur Mikrostrukturtechnik
Forschungszentrum Karlsruhe
Hermann-von-Helmholtz-Platz 1
76344 Eggenstein-Leopoldshafen
Germany

S. Achenbach
Institut fur Mikrostrukturtechnik
Forschungszentrum Karlsruhe
Hermann-von-Helmholtz-Platz 1
76344 Eggenstein-Leopoldshafen
Germany

P. Meyer
Institut fur Mikrostrukturtechnik
Postfach 3640
76021 Karlsruhe
Germany

R. Lawes
CCLRC Rutherford Appleton Laboratory
Central Microstructure Facility
Chilton
DIDCOT OX11 0QX
United Kingdom

1415 J. C. Barbour, 1112
1415 T. A. Friedman, 1112
1077 T. E. Zipperian, 1740
0603 J. J. Hudgens, 1743
0603 T. Lemp, 1743
0603 W. C. Sweatt, 1743
1425 W. G. Yelton, 1743

0877 M. J. Cieslak, 1800
Attn: R. J. Salzbrenner, 1801
G. S. Heffelfinger, 1802
0340 A. Hall, 1832
0889 J. S. Custer, 1851
0889 T. E. Buchheit, 1851
0889 M. T. Dugger, 1851
0889 S. V. Prasad, 1851
0865 D. L. Cook, 1900
0437 C. L. Knapp, 2120
0503 D. W. Plummer, 2330
0319 J. R. Fellerhoff, 2610
0311 M. J. Craig, 2613
0319 R. E. Kreutzfeld, 2613
0319 G. T. Randall, 2613
1310 E. J. Garcia, 2614
1310 M. A. Polosky, 2614
1310 G. E. Sleefe, 2614
0319 L. L. Lukens, 2618
0319 D. E. Petersen, 2618
0319 C. W. Vanecek, 2618
0196 R. Wild, 2618
9001 M. E. John, 8000
Attn: R. H. Stulen, 8100
K. E. Washington, 8900
9054 W. J. McLean, 8300
Attn: R. W. Carling, 8350
A. E. Pontau, 8358
D. R. Hardesty, 8360
9007 D. R. Henson, 8200
Attn: G. A. Thomas, 8220
W. G. Wilson, 8230
9005 B. K. Damkroger, 8240
9036 R. V. Davalos, 8245
9036 M. A. Forman, 8245
9409 W. C. Replogle, 8245
9403 J. M. Hruby, 8700
9401 G. D. Kubiak, 8750
9401 J. E. M. Goldsmith, 8751
9401 M. A. Hekmaty, 8751
9401 L. L. Hunter, 8751
9401 K. D. Krenz, 8751
9401 M. E. Malinowski, 8751
9401 S. Mrowka, 8751
9401 D. M. Skala, 8751
9401 A. A. Talin, 8751
9042 G. H. Evans, 8752
9042 R. S. Larson, 8752
9042 C. D. Moen, 8752
9042 R. H. Nilson, 8752
9042 S. K. Griffiths, 8752 (10)
9042 R. S. Larson, 8752
9042 A. Ting, 8752
9401 G. Aigeldinger, 8753
9401 D. R. Boehme, 8753
9401 G. F. Cardinale, 8753
9401 J. T. Ceremuga, 8753
9401 J. T. Hachman, 8753
9401 C. C. Henderson, 8753
9401 J. J. Kelly, 8753
9401 D. E. McLean, 8753
9401 A. M. Morales, 8753
9401 F. J. Pantenburg, 8753
9401 T. I. Wallow, 8753
9401 P. C. Y. Yang, 8753
9409 J. R. Garcia, 8754
9409 S. H. Goods, 8754
9409 J. S. Korellis, 8754
9409 W.Y. Lu, 8754
9161 W. R. Even, 8760
9161 D. L. Medlin, 8761
9403 L. A. Domeier, 8762
9161 E. P. Chen, 8763
9402 K. L. Wilson, 8770
Attn: C. H. Cadden, 8772
J. C. F. Wang, 8773
P. A. Spence, 8774
9403 B. E. Mills, 8773
9403 N. Y. C. Yang, 8773
0824 W. L. Hermina, 9110
0826 J. E. Johannes, 9113
0834 S. N. Kempka, 9113

9018 Central Technical Files, 8940-2
0899 Technical Library, 4916
9021 Technical Communications, 8528
9021 Technical Communications, 8815
for DOE/OSTI